

Damage Detection of Cyclically Loaded Concrete Shear Wall using EMI Technique

A. Likhith Reddy¹, Shirleen Charles¹, C. Bharathi Priya², G.V. Rama Rao²,
N. Gopalakrishnan^{3,4} and A. Rama Mohan Rao³

Abstract: Details of the investigations on an unexplored application of Electro Mechanical Impedance (EMI) technique using smart piezoelectric (PZT) sensors for damage detection of concrete shear wall structures under crack opening and closing is presented in this paper. The behavior and the ability of this method to detect damages, in a heterogeneous quasi-brittle material is studied for its effective utilization in structural health monitoring. The paper discusses the experimental investigations conducted on a concrete shear wall using PZT patches. Conductance data is acquired at different applied lateral displacements of shear wall. Damage index is calculated using Root Mean Square Deviation (RMSD), Mean Absolute Percentage Deviation (MAPD) and Correlation Coefficient (CC) computed between pristine and damaged states. It is found that compared to a metallic specimen, concrete specimens do not show a large variation in these damage metrics, due to reduced modal density and high damping. However, results and observations from these experimental case studies establish that EMI signature from surface bonded PZTs can identify damages even for a heterogeneous material like concrete, with improved and modified damage metrics.

Keywords: Electromechanical Impedance (EMI), Admittance, Piezoelectric effect, Root Mean Square Deviation (RMSD), Damage detection, Mean Absolute Percentage Deviation (MAPD) and Correlation coefficient (CC).

1 Introduction

Civil engineering infrastructure is one of the most expensive national investment and asset of any country as it facilitates country's economic development. Hence

¹ Research Student. CSIR-Structural Engineering Research Centre, Chennai, India.

² Scientist. CSIR-Structural Engineering Research Centre, Chennai, India.

³ Chief Scientist. CSIR-Structural Engineering Research centre, Chennai, India.

⁴ Corresponding author. Email: ng@serc.res.in; gnrmana68@gmail.com

it is important to continuously maintain and monitor the strength and serviceability condition of buildings and structures for effective load transmission. Presence of damages like cracks have to be identified and quantified in order to assess the condition of a structure. For important structures like bridges, condition monitoring is vital especially after occurrence of natural hazards like earthquake, cyclones etc. In recent years, the structures are monitored using “smart” materials using specialised algorithms and techniques. The smart sensing techniques provide efficient continuous monitoring in economical ways. The piezoelectric sensors (PZT) is one such smart sensing technologies that can be used for condition monitoring of any structure. PZTs are capable of acting as both sensor and actuator. When a PZT patch attached to a structure is driven by a fixed, alternating electric field of high frequency, a small deformation is produced in the PZT patch and the attached structure. The response of this mechanical vibration is transferred back to the PZT patch in the form of an electrical response. When a crack or damage causes change of the mechanical dynamic response, it is manifested in the form of an electrical impedance response of the PZT patch. This principle can be widely exploited in smart SHM techniques.

The EMI technique has been widely accepted as a cost effective and sensitive technique for SHM and non-destructive evaluation (NDE) of a variety of engineering systems. An excellent treatise on the wave propagation mechanism, EMI techniques and constituting relationships is found in the book by Giurgiutiu [Giurgiutiu (2008)]. The structural element to be monitored is instrumented with a PZT patch on the surface, and is excited through an alternating voltage signal using an impedance analyser/LCR meter, sweeping through a particular frequency range (of the order of tens to hundreds of kilo-Hertz). At any particular frequency, the patch actuates the structure and the structural response is simultaneously sensed and measured by the patch in terms of electromechanical admittance (a complex numbered reciprocal of impedance), consisting of conductance (real component), and susceptance (the imaginary component). The real part of the EMI also reflects the point wise mechanical impedance of the structure, and the EMI spectrum is equivalent to the point wise frequency response of the structure. As damage (a crack, corrosion, de-bonds) develops in the structure, the point wise impedance in the vicinity of damage changes. Piezoelectric active sensors placed at critical structural locations will be able to detect these near-field changes. In addition, due to the sensing localization property of this method, far-field influences will not be registered in the EMI spectrum. Owing to the high frequency of excitations (30–400 kHz range), the damage sensitivity of the EMI technique is comparable to other ultra-sonic based NDE techniques.

Generally each PZT sensor has its own area of influence. This area is characterized

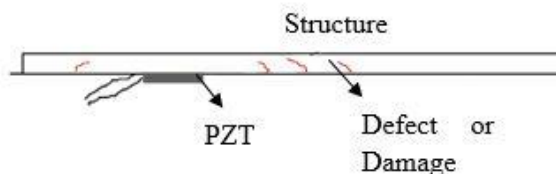


Figure 1: PZT patch acting as active sensor to monitor structural damage.

by a sensing radius and the corresponding circle. As the sensing radius increases, the capability of sensor detection asymptotically decreases. Damage within the area of influence of the sensor is highly sensitive as it creates higher disturbances than the damage outside the area of influence. In order to sense all the damages, overlapping of sensing circles can be done such that presence of cracks, corrosion, and de-bonds/ delamination can be effectively detected (Fig 1) .

The present study is undertaken towards bridging the knowledge gap due to the lack of adequate research and literature available on EMI based studies on concrete structure. The main objectives of the present study include: (1) To obtain the EMI signatures of the four patches in pristine state and damaged state (damage is quantified by increased post-elastic displacement of shear wall, associated with residual permanent set) thereby comparing them and obtaining the damage index. (2) Relating crack width with the damage metrics: RMSD and CC. (3) Checking the signatures for repeatability and re-computing the damage metrics. (4) Finding the correlation between pristine and subsequent damaged states.

2 Background and Literature Review

There are many approaches available for damage quantification. The literature related to damage diagnostics is quite extensive and therefore this section is not intended to be a complete literature survey on the field. Instead, a brief summary of approaches and corresponding damage metrics has been provided. Liu et al. (2013) in their comprehensive study have reported the detection and identification of structural cracks emanating from rows of rivet holes in thin metallic plates using lamb waves using a PZT active sensing network. The diagnosis is carried for crack detection and crack localization using both simulation data and experimental data. Lim et al. (2011) have reported the possible improvements on damage detectability using PZT sensors under varying temperature and external loading conditions and to minimize false-alarms due to these variations. Park et al. (2011) have exhaustively studied cross correlation (CC) based data analysis to quantify the changes in impedance measured at the PZT patches due to the de-bonding condi-

tions that occur in a CFRP laminated concrete surface. Lakshmanan et al. (2008) and Raghuprasad et al. (2008) proposed wavelet and radial basis function (ANN) based damage identification from dynamically measured parameters. Lakshmanan et al. (2009) also proposed a smeared damage model and the sensitivity matrix of static deflection due to damage (reduction of flexural EI) formulated and solved as an over-determined sets of equation.

2.1 Basic Electromechanical equations

Piezoelectric patches typically develop surface charges under mechanical stresses and conversely undergo mechanical deformations when subjected to electric fields, as expressed mathematically by Eq. 1 & Eq. 2.

$$D_i = \epsilon_{ij}^T E_j + d_{im} T_m \tag{1}$$

$$S_k = d_{jk} E_j + s_{km}^E T_m \tag{2}$$

where D_i =Electric Displacement; S_k = mechanical strain; E_j =electric field; and T_m =mechanical stress. ϵ_{ij}^T denotes the complex electric permittivity of the PZT material at constant stress; d_{im} and d_{jk} =piezoelectric strain coefficients (or constants); and s_{km}^E =complex elastic compliance at constant electric field. The superscripts “T” and “E” indicate that the quantity has been measured at constant stress and constant electric field, respectively. Fig.2 show the modeling of the host’s structural impedance Z_s connected to the PZT patch at the end, with the patch undergoing axial vibrations under an alternating electric field E_3 .

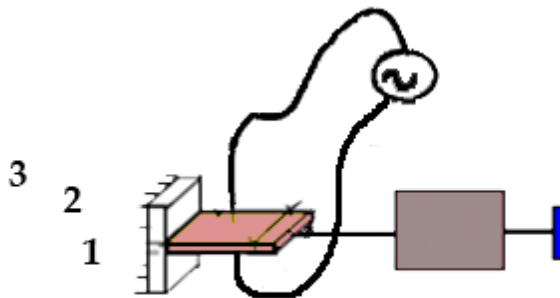


Figure 2: Model of the host structure with mechanical impedance Z_s connected to the PZT patch.

The electromechanical admittance consists of the real and imaginary part which depends on the properties of PZT and structure. This two dimensional governing equation is expanded by Bhalla and Soh (2004), and is given in Eq. 3.

$$\bar{Y} = G + B_j = \omega j \frac{l^2}{h} \left[\bar{\epsilon}_{33}^T - \frac{2d_{31}^2 \bar{Y}^E}{(1-\nu)} + \frac{2d_{31}^2 \bar{Y}^E}{(1-\nu)} \left(\frac{Z_{a,eff}}{Z_{s,eff} + Z_{a,eff}} \right) \bar{T} \right] \quad (3)$$

Where, \bar{Y}^E is the electrical admittance (inverse of electrical impedance) across the PZT terminals; w , l , and h represent the PZT patch’s dimensions; ν is the Poisson’s ratio of PZT patch; d_{31} =piezoelectric strain coefficient for the 1–3 axes; and ω =angular frequency. $\bar{Y}^E = Y^E(1+\eta_j)$ =complex Young’s modulus of the PZT patch (at constant electric field) and $\bar{\epsilon}_{33}^T = \epsilon_{33}^T(1-\delta_j)$ the complex electric permittivity (at constant stress), with the symbols η and δ denoting the mechanical loss factor and the dielectric loss factor respectively. \bar{T} is the complex tangent ratio, which in an ideal situation would be equal to $\tan(\kappa l)/\kappa l$. $Z_{s,eff}(\omega)$ and $Z_{a,eff}(\omega)$ are the effective structural and mechanical impedances. It can be observed that these two terms combine to couple the impedances of the structure and the piezoelectric patch. This coupling allows one to measure the mechanical impedance of the structure through the electrical impedance of the piezoelectric patch. The expression for $Z_{a,eff}$ in terms of complex Young’s modulus and Poisson’s ratio of PZT patch is given Eq. (4).

$$Z_{a,eff} = \frac{2h\bar{Y}^E}{j\omega(1-\nu)\bar{T}} \quad (4)$$

Where κ =wave number related to the density ρ , complex Young’s modulus Y^E of the patch. For the one dimensional case, the wave number is defined in Eq. (5).

$$\kappa = \omega \left[\frac{\rho}{\bar{Y}^E} \right]^{0.5} \quad (5)$$

The wavelength of the signal used to detect damage of a given size must be smaller than the characteristic length of the damage. The frequency range of 30-400 kHz is selected through trial and error, to satisfy this requirement and detect incipient damage. The sensitivity of EMI method is influenced by many factors like PZT excitation voltage, the distance between damage and sensor etc. Hence, these parameters are to be considered carefully. In addition, the maximum frequency considered should be less than 500 kHz. Because of the above reasons and the high frequency of excitation, the sensing region is very small and the obtained conductance signatures are more sensitive to the piezoelectric patch and its bonding conditions and not of the structure [Park et al. (2009)]. However, maximum

frequency can be below this value based on the material of host structure. The limitations of the EMI method reside in its sensing localization which limits its application to near field damages [Zagrai and Giurgiutiu (2001)]. Boundary Element Method (BEM) to investigate the influence of output voltage on the shear related to three-dimensional damage of solids, the presence of the adhesive layer and the elastic interaction between the patch itself and the host elastic substrate is extensively studied by Benedetti, Milazzo and Aliabadi (2009). Box-Behnken design of experiment (simulation) technique to relate damage parameter such as stiffness reduction to the electromechanical admittance signature generated by piezoelectric sensors at specific frequency ranges has been investigated by Providakis and Voutetaki (2007).

3 Experimental Investigations

The behavior and the ability to detect damages, of the piezoelectric patches, in a heterogeneous material is studied for its utilization in SHM. For this, several experiments are conducted on concrete structures. All the tests are conducted at room temperature under same temperature and humidity conditions. The details of the experiments and results obtained are discussed in the following case study. In all cases the piezoelectric patches are surface bonded to the structure.

3.1 Case Study :*Experimental studies on PZT bonded concrete shear wall*

The experimental study had been performed on a concrete shear wall which is 1:4 scale of the prototype. Fig.3(a) shows the experimental setup for the cyclic load test on shear wall. The dimensions of shear wall specimen are 3 m height, 1.56 m width and 0.2 m thickness. The shear wall is axially loaded with a super-imposed vertical load of 160 kN. Displacement controlled cyclic loading test is applied on the shear wall. The base of the shear wall is fixed and displacement is given at the top of the shear wall using a hydraulic jack. Displacement is an in-direct quantification of loading, during elastic phase of a concrete structure. Generally for quasi brittle structures and ductile structures with steeply falling hysteretic structures, displacement controlled tests are performed on the structure, so as to capture the post-peak force-displacement hysteretic characteristics. Load controlled tests are generally not preferred. Applied displacements are indicators of the increased crack width, crack length and permanent set of a structure. Cyclic loads are applied through a push-pull hydraulic jack connected by a pinned connection to the steel box encasing the top slab. Initially the load is applied as push, till the monitored displacement has reached the peak displacement. Then the un-loading is done and the shear wall is pulled in the other direction, such that the negative peak displacement of the cycle is reached. Then it is slowly un-loaded until the load is zero. This completes



Figure 3(a): Experimental setup for the cyclic load test on shear wall.



Figure 3: (b) Experimental setup and (c) Location of for PZT patches.

one cycle. Three cycles of loading for each peak displacement of 2, 4, 6, 8, 10, 15, 20, 25, 30, 40 and 50 mm are applied on the shear wall. The experimental setup consists of an LCR meter, a notebook computer and 4 PZT patches surface bonded on the shear wall as shown in Fig 3 (b) and Fig 3(c). PZT patches are bonded to the bottom of the shear wall with epoxy resin. Baseline signatures are acquired from the four patches in the undamaged state. A displacement of 2 mm had been given to the structure by the hydraulic jack and the conductance signature for the four patches is acquired. Similarly the signatures are acquired for all cases of displacements increasing up to 60 mm. This corresponds to a lateral drift of 2% of the wall height, which is close to an incipient damage state of the wall. Crack opening and closing is clear apparent in the experimentally obtained hysteresis curves (Fig. 4). The crack closure of a previously opened-up crack is seen through the increase in stiffness of the shear wall. The trajectory of the hysteresis loop as it touches the negative Y-axis where the crack closes results in a sudden gain of strength.

In order to select a suitable frequency range for acquiring the admittance signatures, the transducers on the first specimen are scanned over a wide frequency range of 150–1000 kHz. Optimal frequency range is selected to cover large number of dominant modes and to have a high modal density so as to ensure high sensitivity to the damage. More peaks are found in 150-350 KHz range. Hence, in this case the optimal frequency is obtained to be 200-300 KHz.

3.2 Results and discussions – Case Study

Figures are plotted between the frequency and conductance for all patches. Marginal variations are observed between the conductance signatures corresponding to pristine state and the damaged state. This is due to the reduced modal density and lack of metallic ringing modes as normally seen in metallic structures. As patch 4 is near to damage, the conductance signature shows greater variation compared to patch 1 as observed from Fig 5(a) and 5(b).

3.3 Damage Quantification Indices (Damage metrics)

Damage in civil structures are quantified by the appearance of cracks, elongation of cracks, increased crack widths and permanent set (after un-loading) manifesting in the form of sudden lack of stiffness of the structure. However EMI catches up with the local loss of stiffness arising near the vicinity of the damage. The subsequent section describes the various damage metrics and discusses the relative merits of each and also the changes in each as the damage progresses.

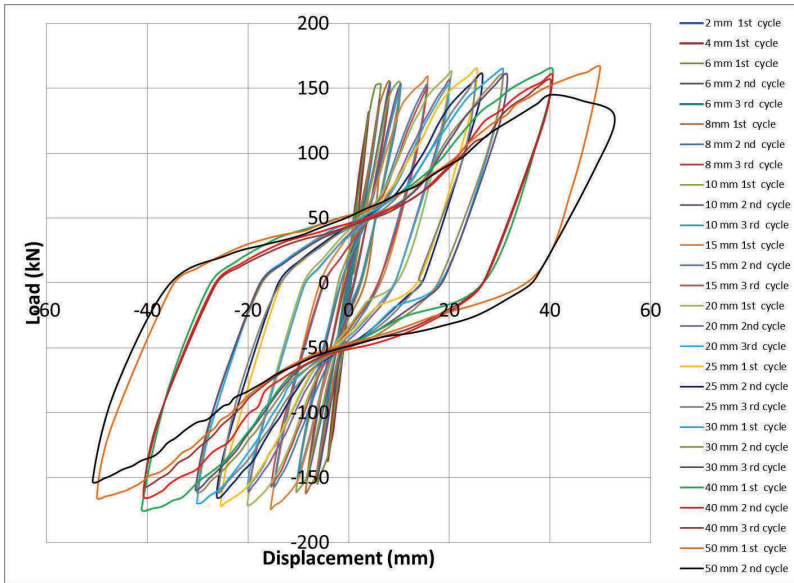


Figure 4: Hysteretic behaviour of shear wall obtained in cyclic load test depicting strength & stiffness degradation and pinching.

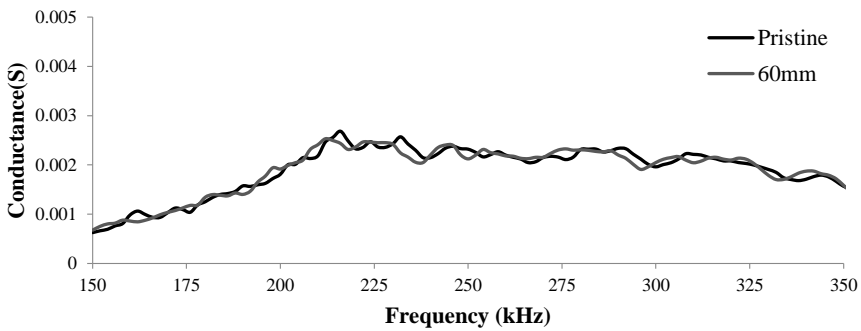


Figure 5(a): Conductance signature of patch1 for pristine and 60mm top displacement of shear wall.

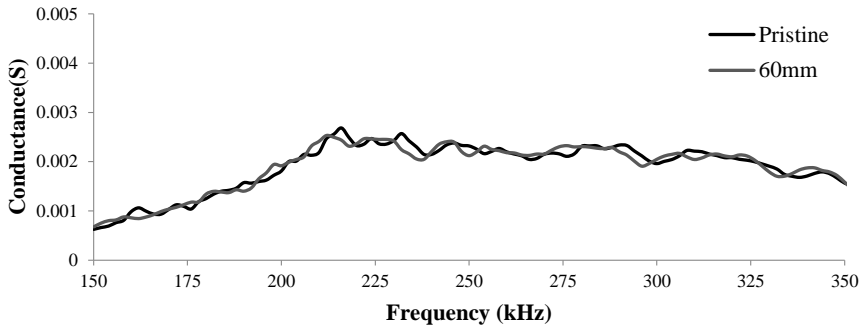


Figure 5(b): Conductance signature of patch4 for pristine and 60mm top displacement of shear wall.

3.3.1 Root Mean Square Deviation (RMSD) Index

In impedance method for structural health monitoring, the key indicator of damages is the change in the conductance signatures of the bonded PZT transducer. Although this change can be observed visually, it is necessary to adopt suitable statistical techniques to quantify it. Samman and Biswas (1994a, 1994b) presented a few pattern recognition techniques such as signature assurance criteria (SAC), waveform chain code (WCC) technique and adaptive template matching (ATM) to quantify similar changes in acceleration signatures for a bridge structure. Giurgiutiu and Rogers (1998) used the root mean-square deviation (RMSD) between the signatures of the two states as the suitable damage index. Bhalla (2005) in an excellent study on detection and characterization of damage in concrete cubes, compared the above techniques and observed that the RMSD between the signatures was the most suitable damage index to characterize structural damage. Hence in the present study RMSD is used to quantify the damage. RMSD is computed using equation (6).

$$\text{RMSD} = \frac{\sqrt{\sum_{j=1}^N (G_j^1 - G_j^0)^2}}{\sqrt{\sum_{j=1}^N (G_j^0)^2}} \quad (6)$$

G_j^1 - post-damage conductance at the j-th measurement frequency and G_j^0 - corresponding pre-damage value.

It can be observed from Table 1 that for 150-250 KHz and 250-350 KHz range, patch 2 which is far from damage than patch 3 and 4 is showing higher RMSD

Table 1: RMSD variation for different frequency ranges.

Frequency Range (in KHz)	RMSD (%)			
	Patch 1	Patch 2	Patch 3	Patch 4
150-250	6.285	13.341	11.632	19.694
250-350	3.633	12.394	10.576	10.424
200-300	5.271	7.493	12.559	12.921

Table 2: RMSD variation with top displacement of shear wall for frequency range 200-300 kHz.

Top Displacement of Shear wall,mm	(RMSD) %			
	Patch 1	Patch 2	Patch 3	Patch 4
2	2.086	0.752	0.974	5.104
4	3.219	1.277	3.444	6.877
10	4.510	1.934	6.422	7.823
15	4.930	2.517	6.840	9.099
20	4.984	2.737	6.529	7.666
25	5.362	2.890	6.381	8.645
30	5.772	3.024	5.195	6.702
40	5.308	3.075	7.055	12.299
60	5.725	3.298	11.671	11.985

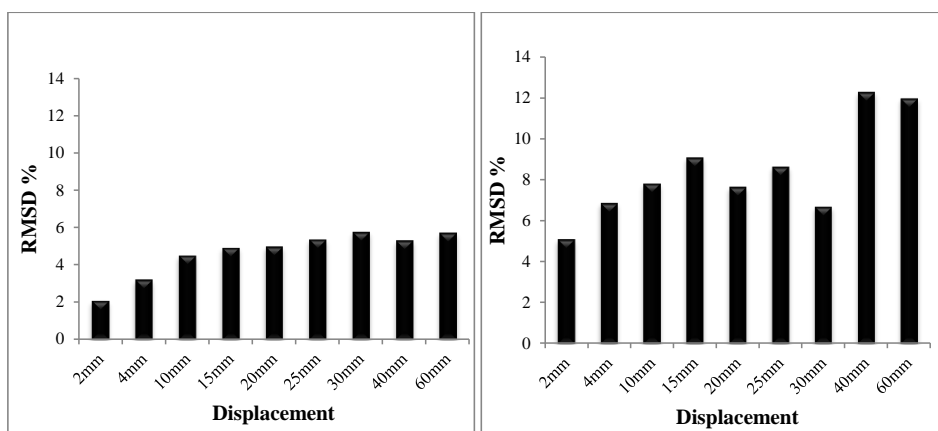


Figure 6: Displacement vs. RMSD plots for patch 1 and 4.

value. But in 200-300 KHz frequency range patch 1 and 2 show lower RMSD than patches 3 and 4 as expected. Hence, frequency range of 200–300 kHz is chosen as the desired range for the current study. These signatures consist of a total of 201 data points, with dominant peaks seen and observed in this range. For every state, either pristine or damaged, two signatures for each patch are acquired and an average signature is worked out to ensure repeatability.

The RMSD plots shown in Fig.6 clearly indicate the propagation of the damage with increasing displacement which is sensed well by the PZT patches. Table 2 shows the RMSD values of all the 4 patches with increasing displacement in 200-300 KHz frequency range. As patches 3 and 4 are near to damage, the RMSD values computed between conductance signature of pristine state and subsequent damage states at 2mm, 4mm etc. are almost double the RMSD values obtained for patch 1 and are shown in Fig.6.

3.3.2 Mean Absolute Percentage Deviation (MAPD)

From the experimental results, it may be seen that the mode density for a typical range of 10 kHz is less for a non-homogeneous material like concrete as compared to a metallic specimen. Hence other damage metrics than just RMSD are investigated and compared so as to recommend and select an appropriate damage index. Mean absolute percentage deviation (MAPD), Covariance (COV) and correlation coefficients (CC) are computed out of the admittance signatures between pristine and damage states and compared. Existing research data is available to a large extent as metallic structures and scarcely seen for large scale reinforced concrete structures.

The MAPD between the two signatures x_i and y_i ($i= 1,2,3 \dots N$) is computed using equation (7).

$$\text{MAPD} = \frac{100}{N} \sum_{i=1}^N \left| \frac{y_i - x_i}{x_i} \right| \quad (7)$$

The MAPD index is similar to RMSD as it evaluates the average of the deviations at each individual data point of the signatures (Table 3).

As patch 4 is near to damage, the MAPD values computed between conductance signature of pristine state and subsequent damage states at 2 mm, 4 mm etc. are almost double the RMSD values obtained for patch 1(Fig 7). It can be observed that MAPD and RMSD are giving similar results as expected.

3.3.3 Covariance

Covariance evaluates the averaged product of the deviations of admittance signature data points from their respective means. Mathematically, covariance is evaluated

Table 3: MAPD variation with top displacement of shear wall for frequency range 200-300 KHz.

Top Displacement of Shear wall, mm	Mean Absolute Percentage Deviation (MAPD) %			
	Patch 1	Patch 2	Patch 3	Patch 4
2	1.760	0.583	0.811	5.794
4	2.699	0.911	2.719	7.668
10	3.697	1.613	4.942	8.863
15	3.986	2.203	5.231	6.316
20	3.773	2.348	4.956	8.274
25	4.070	2.612	5.583	6.055
30	4.502	2.894	4.382	7.578
40	4.058	3.052	5.198	15.871
60	4.499	3.112	9.700	13.814

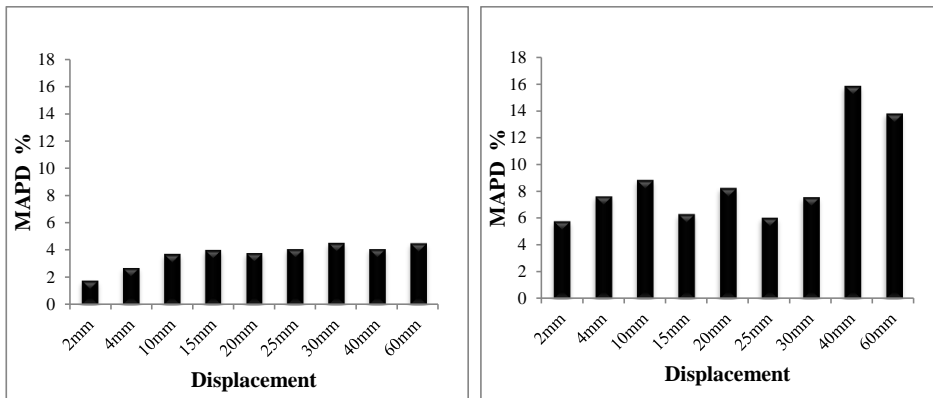


Figure 7: Displacement vs. MAPD plots for patch 1 and 4.

using equation (8).

$$\text{COV}(x,y) = \frac{1}{N} \sum_{i=1}^N (x_i - \bar{x})(y_i - \bar{y}) \quad (8)$$

where \bar{x} and \bar{y} are the mean values of the two sets of data from the admittance signatures. Covariance is a measure of how much two signatures change together. If both the signatures move together, positive covariance is obtained and vice versa. When values in both signatures are unrelated, covariance approaches zero. Thus, if the covariance is more close to zero the signature deviates a lot and presence of damage can be quantified.

3.3.4 Correlation Coefficient

The Correlation Coefficient (CC) is equal to the covariance of two signature data sets divided by the product of their standard deviations.

$$cc = \frac{\text{Cov}(x,y)}{\sigma_x \sigma_y} \quad (9)$$

Where, σ_x and σ_y are standard deviations of the signature datasets x and y , respectively. The CC measures the linear relationship between two signatures in a manner similar to covariance, with the only difference being that it is scaled to be independent of the unit of measurement. The CC is positive, negative or nearing zero according to the correlation between the values of the two data sets. The value of the CC is 1, when for all the peaks in the pristine state signature and the damaged state signature coincide at the same frequency. When the CC is -1, it indicates that, at all the frequencies where the pristine state signature had peaks, the damaged state signature has valleys, and vice versa. Thus, lower the value of the CC, the larger the deviation in the signatures, indicating a greater degree of damage.

The Correlation coefficient variation with increasing top displacement of shear wall ranging from 2 mm to 60 mm is shown in Table 4. The shear wall reached closer to its ultimate displacement at 60 mm of imposed lateral displacement.

The correlation coefficient values are decreasing with increasing damage level as expected. This decrease is pronounced in case of patch 4 which is closer to major crack zone. Fig.8 shows the decreasing trend of the correlation coefficient with increasing top displacement of shear wall.

Here, R^2 is the correlation coefficient of datasets x , y . It has been found from Fig.9 that increase in the power of correlation coefficient increases the gap between the initial small displacements of shear wall and the later large displacements. Even though such a magnification of difference through higher powers is reported by

Table 4: Correlation coefficient variation with top displacement of shear wall.

Top displacement of Shear wall, mm	Patch 2	Patch 4
2	0.999	0.990
4	0.998	0.982
10	0.997	0.977
15	0.995	0.968
20	0.994	0.977
25	0.994	0.971
30	0.993	0.983
40	0.993	0.950
60	0.993	0.952

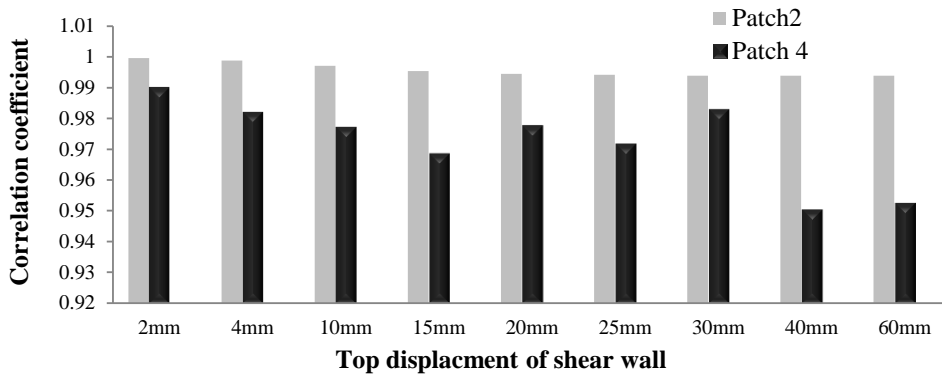


Figure 8: Displacement vs. CC plots for patch 2 and 4.

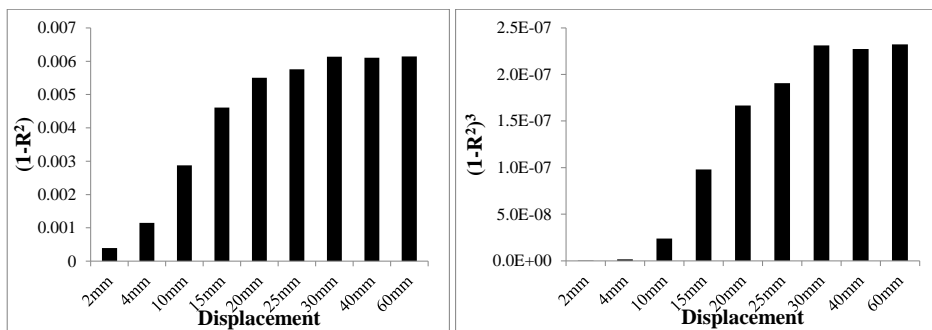


Figure 9: (1-R²) and (1-R²)³ variation with top displacement (in mm) for patch 2.

Giurguitiu (1994a), Park (2006) and other researchers, the extension to concrete structure is not adequately available. This helps in clearly identifying damage after significant permanent set has occurred in the shear wall. In case of fourth order of correlation coefficient, the damage index value of 10 mm is found to reduce drastically when significant permanent set has occurred. Hence, third power of the correlation coefficient deviation $(1-R^2)^3$ is a good damage indicator [Seunghee et al. (2011)], which tends to increase linearly with increase in the top displacement of shear wall.

It can be observed that MAPD and RMSD are giving similar results as expected. Covariance (COV) and CC values progressively decrease with the increase in damage extent, as expected. The index values at zero refer to the undamaged state COV and CC evaluated for the pristine state signature with respect to itself. The COV and CC indices are also capable of detecting increase in damage extent, although not as clearly as the RMSD and MAPD indices.

3.4 Effects of Crack Opening and Closure Displacements on Conductance Signatures

Crack width for concrete structures is synonymous with crack mouth opening displacements in fracture mechanics terminology. Experimental study is conducted for measuring the effect of crack opening and closure of the shear wall in push, pull and neutral condition. For this reason, the shear wall had been initially pushed for a displacement of 15 mm and conductance signature is taken and the shear wall is brought to neutral position. Then, the shear wall was pulled for a displacement 15 mm and conductance signature is taken again. Similar procedure is implemented for 30 mm displacement of shear wall. The change in RMSD (Table 5) and CC values (Table 6) of patches 1 and 3 are used to explain the phenomenon of crack opening and crack closure.

Table 5: RMSD variation with top displacement of shear wall.

Patch	G-15 mm (Push)	G-15 mm (Pull)	G-15 mm (Neutral)	G-30 mm (Push)	G-30 mm (Pull)	G-30 mm (Neutral)
1	5.187	4.681	4.930	5.532	4.819	5.772
3	3.714	6.921	6.840	5.784	7.232	5.892

In push condition crack opening takes place on patch 1 side of shear wall, and crack closure on patch 3 side. This phenomenon is reversed in pull condition. The RMSD of patch 1 in push condition is higher than its pull condition and CC is low for push condition compared to pull condition. This is attributed to the crack

Table 6: Correlation coefficient (CC) variation with top displacement of shear wall.

Patch	G-15 mm (Push)	G-15 mm (Pull)	G-15 mm (Neutral)	G-30 mm (Push)	G-30 mm (Pull)	G-30 mm (Neutral)
1	0.750	0.826	0.762	0.706	0.805	0.665
3	0.991	0.978	0.971	0.979	0.968	0.985

opening on patch 1 side as it is responsible for higher RMSD and lower CC in push condition compared to pull condition. In pull condition, crack closure is expected on patch1 side and therefore it explains the reason for lower RMSD of patch 1 in pull condition. Whereas, RMSD of patch 3 in push condition is lower than pull condition. RMSD and CC values are consistent in explaining the push-pull effect.

3.4.1 Comparison of Admittance Signatures on Crack Opening Displacements (COD)

Increasing crack width is a measure of damage state in a structural system. Eight LVDTs are placed to capture the crack pattern. The position of LVDTs is shown in the Fig 10. Piezoelectric patches are on the opposite side of the shear wall. The crack width information from LVDTs 1, 2 5 and 6 are used to plot graphs between crack width and RMSD values. Similar figures are plotted to observe the CC variation with increasing crack width.

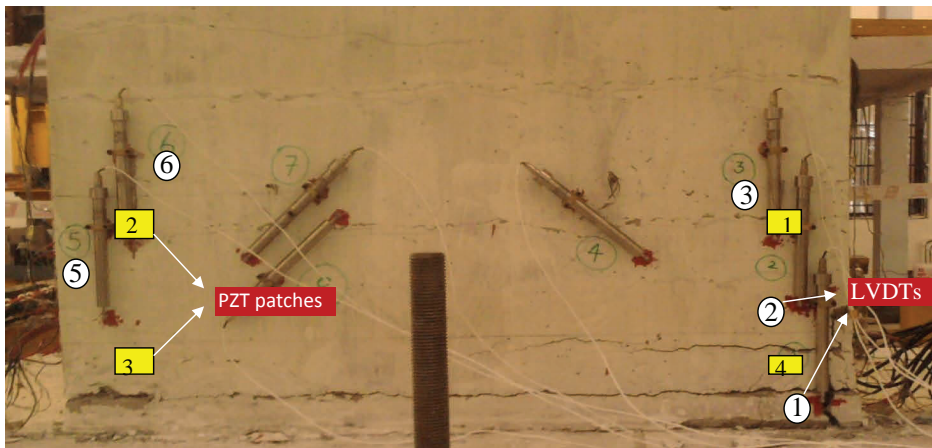


Figure 10: Position of LVDTs on the shear wall with 20mm cycle.

The LVDTs are on the front face of shear wall which are indicated by circles with

white background in Fig. 10. PZTs are located on the back face of shear wall at 20 cm and 50 cm from the bottom of the toe and 40 cm clear cover. PZT are indicated by squares with yellow background. With increasing crack width, the RMSD values are expected to increase, which can be noted from the graphs shown in Fig 11a to 18b. CC values are decreasing with increasing crack width as expected. LVDT 1 captured the major cracks showing significant crack width.

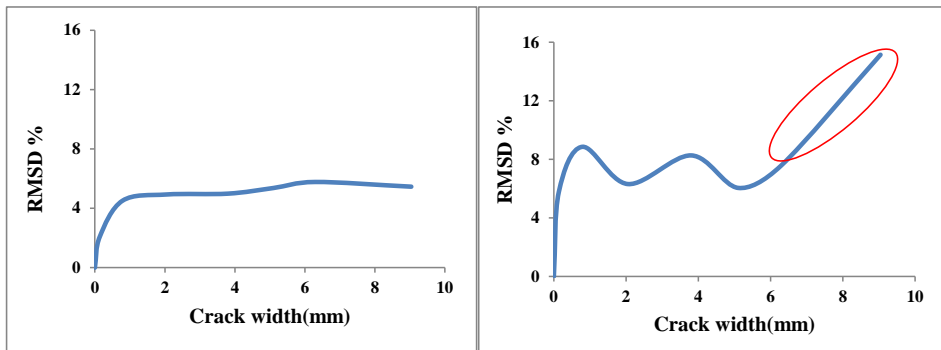


Figure 11: (a) RMSD variation of patch 1 and (b) patch 4 versus crack opening data from LVDT 1.

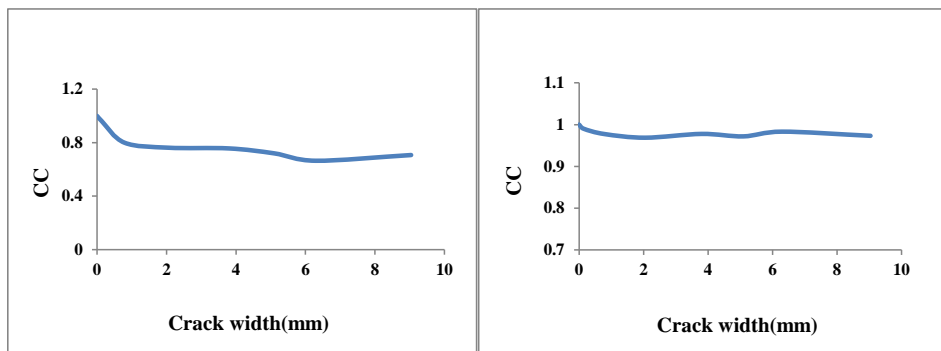


Figure 12: (a) CC variation of patch 1 and (b) patch 4 versus crack opening data from LVDT 1.

LVDTs 3, 4 are relatively far from major damage, when compared with LVDTs 1, 2. Sudden spurt in RMSD values and sudden fall in the correlation coefficient values as indicated in these figures can be attributed to the abrupt loss of stiffness of the shear wall at 60 mm displacement. Also, there is abrupt increase in the RMSD values for patches 3, 4 due to the same reason.

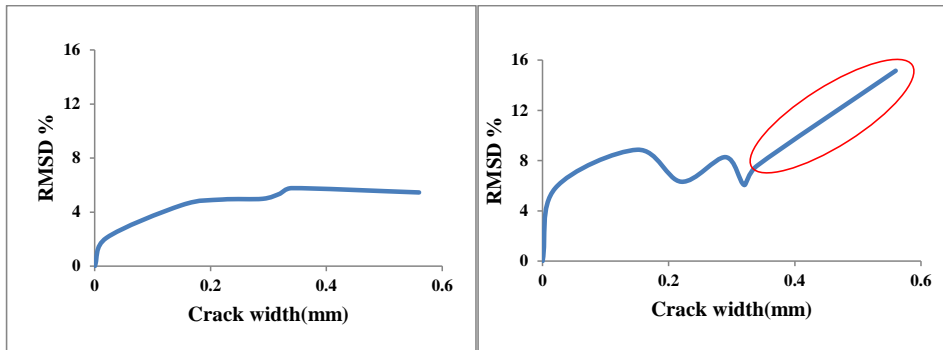


Figure 13: (a) RMSD variation of patch 1 and (b) patch 4 with crack opening data from LVDT 2.

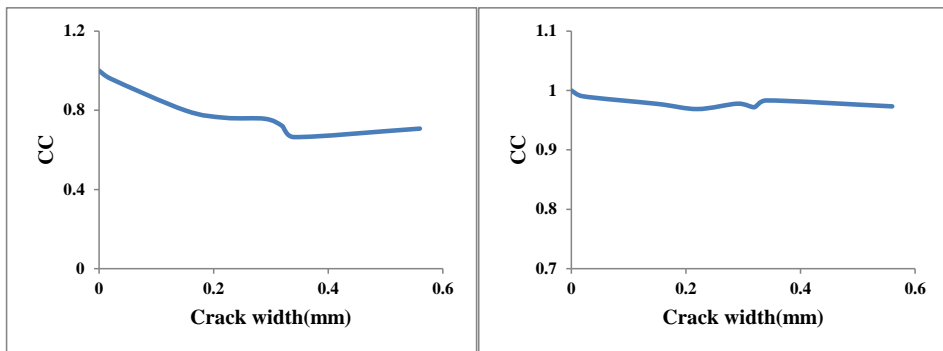


Figure 14: (a) CC variation of patch 1 and (b) patch 4 with crack opening data from LVDT 2.

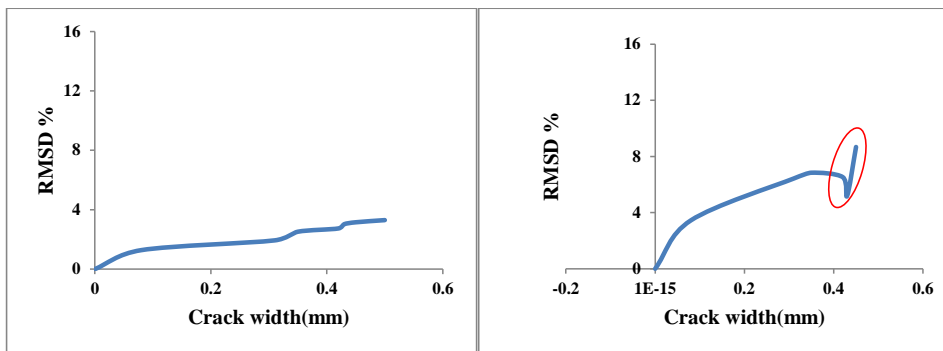


Figure 15: (a) RMSD variation of patch 2 and (b) patch 3 with crack opening data from LVDT 5.

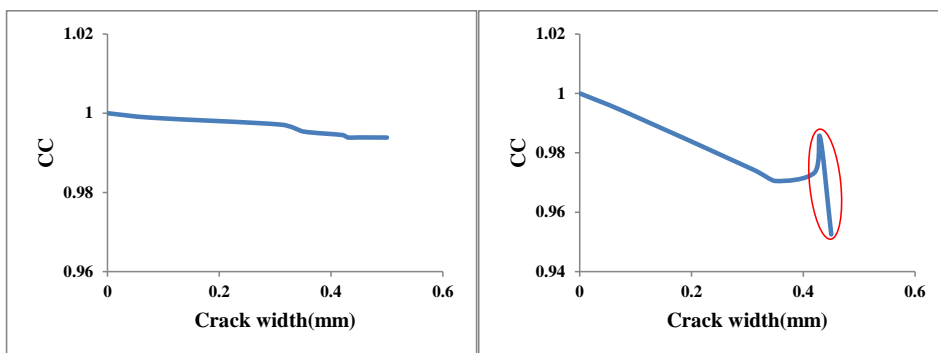


Figure 16: (a) CC variation of patch 2 and (b) patch 3 with crack opening data from LVDT 5.

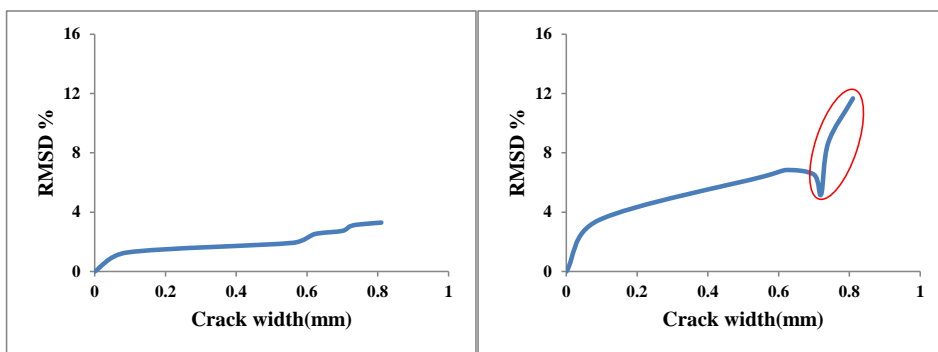


Figure 17: (a) RMSD variation of patch 2 and (b) patch 3 with crack opening data from LVDT 6.

4 Conclusions

Existing wealth of literature does not generally cover much on the damage identification of non-homogeneous concrete specimen using EMI signatures and the present work tries to bridge the knowledge gap in this direction. The application of feature extraction technique from EMI signatures using smart piezoelectric sensors in damage detection of concrete structure for SHM applications is experimentally investigated and presented in this paper. This is a simple approach to locate and quantify damage from the measured signatures of the PZT patches. This can be used to quickly assess the integrity of the critical parts of the structure after a disaster such as an earthquake. Especially, the inaccessible parts of the structure, which are not exposed to visual check, can be easily monitored using the

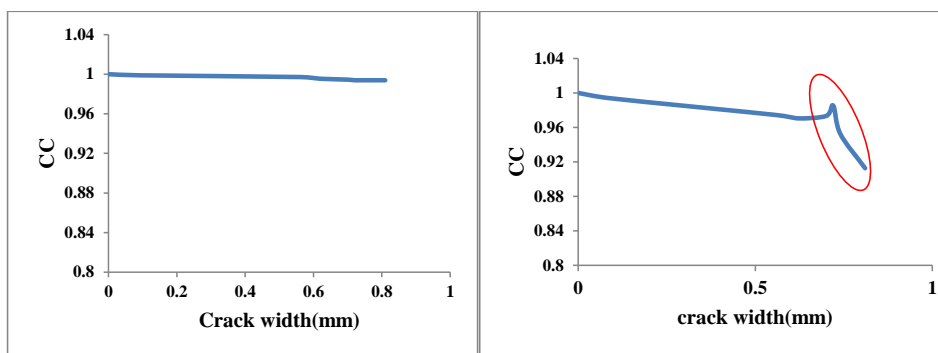


Figure 18: (a) CC variation of patch 2 and (b) patch 3 with crack opening data from LVDT 6.

PZT patches. The studies conducted on shear wall show that damage can be assessed using changes in the conductance signatures obtained from PZT patches. It is observed that for a non-metallic quasi-brittle material like concrete, ultra-sonic localised resonances are generally absent resulting in reduced modal density with highly damped peaks. Consequently, RMSD deviations are magnitude-wise less as compared to a companion metallic specimen. RMSD, MAPD values are found to be very similar and increases linearly with growth of damage. In addition to RMSD and MAPD as damage indices, to magnify the differences between the admittance signatures at pristine and damage states, the correlation coefficient is also computed for all four patches and found to be positively correlated with the baseline (pristine curve). The higher power of $(1-\text{correlation coefficient})$ is found to magnify the differences and is a good damage indicator, which tends to increase linearly with increase in the top displacement of shear wall. This conclusion is already corroborated by Giurgiutiu (2008). Changes in admittance signatures are directly affected by the crack opening displacements of the shear wall structure which are captured by the in-plane LVDTs. All results of correlation coefficient (CC) are found to be consistent with those of RMSD and MAPD. These results indicate that impedance-based damage detection is a promising method for damage detection and a good prognosis tool in the field of structural health monitoring.

Acknowledgement: This paper is being published with the kind permission of the Director, CSIR-Structural Engineering Research Centre, Chennai, India. The fourth author acknowledges the tacit guidance of Guru Ramana and Mahaperiyava.

References

- Benedetti, I.; Milazzo, A.; Aliabadi, M. H.** (2009): Structures with Surface-Bonded PZT Piezoelectric Patches: a BEM Investigation into the Strain-transfer Mechanism for SHM applications. *Structural Durability & Health Monitoring*, vol. 5, no. 3, pp. 251-274.
- Bhalla, S.; Soh, C. K.** (2004): Structural health monitoring by piezo-impedance transducers. Part I: modeling. *Journal of Aerospace Engineering*, ASCE vol. 17, no. 4, pp. 154–165.
- Bhalla, S.; Soh, C. K.; Liu, Z.** (2005): Wave propagation approach for NDE using surface bonded Piezoceramics. *NDT&E International*, vol. 38, pp. 143–150.
- Giurgiutiu, V.; Rogers, C. A.** (1998): Recent advancements in the electro-mechanical impedance method for structural health monitoring and NDE. *Proceedings of Smart Structures and Materials Conference*, Proc. of SPIE, 3329, pp. 536-547.
- Giurgiutiu, V.** (2008): *Structural Health Monitoring with Piezoelectric Wafer Active Sensors*, Academic Press (an Imprint of Elsevier), Burlington, MA.
- Lakshmanan, N.; Raghuprasad, B. K.; Muthumani, K.; Gopalakrishnan, N.; Basu, D.** (2008): Damage evaluation through radial basis function network (RBFN) based artificial neural network scheme. *Smart Structures and System- An Intl Jl.*, vol. 4, pp. 23-49.
- Lakshmanan, N.; Raghuprasad, B. K.; Muthumani, K.; Gopalakrishnan, N.; Basu, D.** (2009): Identification of reinforced concrete beam-like structures subjected to distributed damage from experimental static measurements. *Computers and Concrete- An Intl Jl.*, vol. 4, no. 1.
- Liu, S.; Du, C.; Mou, J.; Martua, L.; Zhang, J.; Lewis, F. L.** (2013): Diagnosis of structural cracks using wavelet transform and neural networks. *NDT & E International*, vol. 54, pp 9–18.
- Lim, H. J.; Kim, M. K.; Sohn, H.; Park, C. Y.** (2011): Impedance based damage detection under varying temperature and loading conditions. *NDT & E International*, vol. 44, no. 8, pp 740–750.
- Park, S.; Kim, J. W.; Lee, C.; Park, S. K.** (2011): Impedance-based wireless de-bonding condition monitoring of CFRP laminated concrete structures. *NDT & E International*, vol. 44, no. 2, pp 232–238.
- Park, G.; Overly, T. G.; Nothnagel, M. J.; Farrar, C. R.; David M. M.; Todd, M. D.** (2006): A wireless active-sensor node for impedance-based structural health monitoring. *Proceedings of US-Korea Smart Structures Technology for Steel Structures*.
- Providakis, C. P.; Voutetaki, M. E.** (2007): Electromechanical Admittance –

Based Damage Identification Using Box-Behnken Design of Experiments. *Structural Durability & Health Monitoring*, vol. 3, no. 4, pp. 211-228.

Raghuprasad, B. K.; Lakshmanan, N.; Gopalakrishnan, N.; Muthumani, K. (2008): Sensitivity of Eigen values to damage and its identification. *Structural durability and health monitoring*, vol. 4, no. 3, pp. 117-144.

Samman, M. M.; Biswas, M. (1994a): Vibration testing for non-destructive evaluation of bridges. I: theory. *Journal of Structural Engineering*, ASCE, vol. 120, no. 1, pp. 269-289.

Samman, M. M.; Biswas, M. (1994b): Vibration testing for non-Destructive evaluation of bridges. II: experiment. *Journal of Structural Engineering*, ASCE, vol. 120, no. 1, pp. 290-306.

Zagrai, A. N.; Giurgiutiu, V. (2001): Electro-Mechanical Impedance Method for Crack Detection in Thin Plates. *Journal of Intelligent Material Systems and Structures*, vol. 12, pp.709-718.

